Trans Indian Inst Met (2017) 70(3):759–768
DOI 10.1007/s12666-017-1081-2

TECHNICAL PAPER

Weldability and Fracture Behaviour of Low Carbon Steel/Aluminium/Stainless Steel Clad Sheet with Resistance Spot Welding

Siva Prasad Murugan[1] · Muralimohan Cheepu[1] · Dae-Geun Nam[2] · Yeong-Do Park[1]

Received: 29 November 2016 / Accepted: 9 February 2017 / Published online: 21 February 2017

Abstract This paper focuses on the resistance spot welding of low carbon steel/aluminium/stainless steel 3-ply clad sheet. Weldability, microstructure, tensile properties and fracture behaviour of the clad sheet with resistance spot welding were evaluated. A "squeeze-out pulse" was used to melt and squeeze out the core aluminium completely from the vicinity of the weld zone before the application of actual welding current. This enabled the clad sheet to be welded without the formation of any Fe–Al intermetallic compound layer in the weld zone. The fracture mode associated with the peel test of the spot weld was used as the criterion for resistance spot weldability evaluation of the clad sheet. A weldability lobe diagram in the welding current–welding time space based on the fracture mode was constructed and it revealed a wide weldable window especially at a welding time of 18 cy. A tensile shear test with a cross head speed of 1 mm/min was conducted to study the tensile strength and fracture behaviour. It revealed four different fracture modes namely button pull, clad-bond fracture, partial thickness-partial clad-bond fracture and interfacial fracture. The nugget size and melting of clad interface and stainless steel layer were the dominant factors in determining the fracture mode.

Keywords Clad sheet · Resistance spot welding · Weldability · Fracture behaviour · Intermetallic compound layer · Clad-bond fracture

✉ Siva Prasad Murugan
msiva048@gmail.com

[1] Department of Advanced Materials Engineering, Dong-Eui University, Busan 47340, Republic of Korea

[2] Transportation and Machinery System Center, Korea Institute of Industrial Technology, Busan 618270, Republic of Korea

1 Introduction

In recent years, the demand for engineering materials to perform a wide verity of functions are increasing. But it is hard to fulfil these requirements with a single metal or alloy. Recently, clad sheets, consisting of layers of dissimilar metals or alloys, have drawn great attention as it can combine the superior properties of the constituent materials [1–3]. For example, an aluminium/steel clad combines the anti-corrosion and thermal properties of aluminium and mechanical properties of steel [4], an aluminium/copper clad offers equivalent electrical and thermal properties of copper with significant weight reduction [5] and magnesium/aluminium clad sheet combines the corrosion resistance and formability of aluminium with high strength-to-weight ratio of magnesium [6]. This study focuses on a 3-ply low carbon steel/aluminium/stainless steel clad sheet which is a candidate material for automotive components and elevator (lift) cabin manufacturing. This 3-ply clad sheet can successfully combine the properties such as low density of aluminium, strength, corrosion resistance and aesthetic surface appearance of stainless steel and low cost and superior weldability of low carbon steel. The application of these 3-ply clad sheets involves welding and joining processes during component manufacturing and assembly. Resistance spot welding is a widely accepted process especially in automotive industry because it is fast, cost effective and suitable for automation [7]. So, the resistance spot weldability of the given clad sheet is an important concern for its successful industrial application.

In the past, several studies have been conducted on the weldability/joinability and mechanical characterization of clad sheets. Laser beam welding of Al/steel clad [4] and steel/stainless steel clad [8], ultrasonic welding of Al/Mg

clad [6], brazing of 3-layer dissimilar Al alloys clad [9] are a few among them. Resistance spot welding and weldability of aluminium and steel with aluminium/steel clad sheet as a transition material has also become the research interests of several researchers. Oikawa et al. [10] and Sun et al. [11] studied the resistance spot welding between aluminium and steel with the usage of aluminium/steel clad sheet as a transition material, and they managed to eliminate/reduce the effect of brittle Fe–Al intermetallic compound layer on the joint properties. However, no studies have been reported till date on the feasibility of resistance spot welding of aluminium/steel or steel/aluminium/stainless steel. Consequently, it is necessary to investigate the resistance spot weldability of steel/aluminium/stainless steel. This paper aims at the resistance spot welding characteristics such as weldability, interface microstructural characterization, mechanical properties and fracture behaviour of a low carbon steel/aluminium/stainless steel 3-ply clad sheet.

2 Materials and Methods

The material used in this study was a three ply clad sheet consisting of low carbon steel (AISI 1008) aluminium (AA 1050) and austenitic stainless steel (AISI 304) of overall thickness 1.3 mm, fabricated by hot rolling process. The chemical compositions of the different constituent materials are provided in Table 1 where low carbon steel, aluminium and stainless steel are designated using LCS, Al and SS respectively. Figure 1 shows the schematic representation of resistance spot welding of the clad sheet with a low carbon steel–low carbon steel interface, using a robot operated servo controlled welding gun with medium frequency DC power source. Hemisphere shaped Cu–Cr electrode with a dome diameter of 6 mm was attached to the welding gun. An electrode force of 300 kgf was used for the welding. The surface of the sample was cleaned with ethyl alcohol to remove oil, dirt etc. Peel test was carried out to evaluate the resistance spot weldability of the discussed material based on the fracture mode. It was a simple shop test in which the spot welds were peeled out using a roller-hand tool and a vice. Tensile shear test with a cross head speed of 1 mm/min was performed to study the mechanical properties and fracture behaviour. The

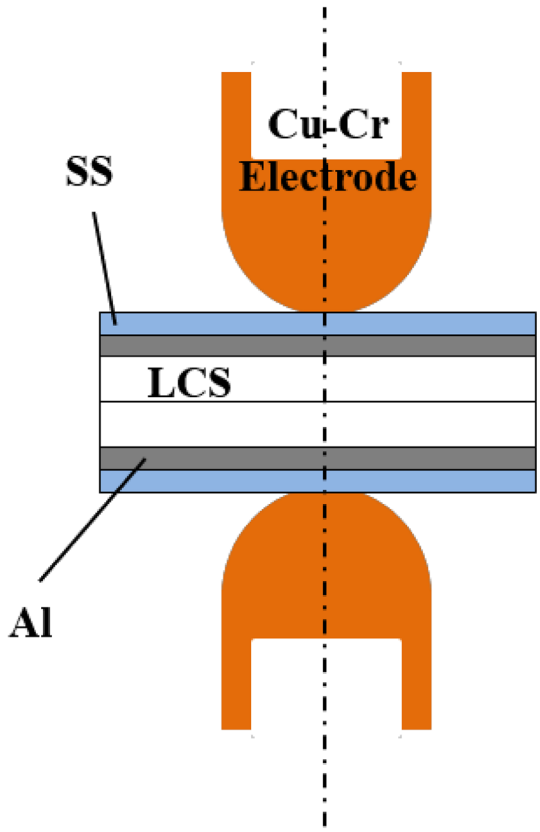

Fig. 1 Schematic representation of resistance spot welding of the clad sheet with a low carbon steel–low carbon steel interface

dimensions of the peel test and tensile shear test samples are shown in Fig. 2. The metallographic analysis was performed using an optical and scanning electron microscope after proper metallographic preparation and chemical etching. An energy dispersive X-ray spectroscopy (EDS) was employed to analyse the elemental distribution.

3 Results and Discussion

3.1 Nugget Formation

The aluminium layer is highly detrimental to the weldability of the clad sheet due to the intermetallic compound layer (IMC) formation and the inherent disparities in chemical, mechanical and thermal properties with that of steel [10–12]. A brittle intermetallic compound layer is

Table 1 Chemical compositions of the different constituent materials (wt%)

Material	C	Si	Mn	S	P	Cr	Ni	Mg	Fe	Al
LCS	0.10	0.50	0.45	0.05	0.04	–	–	–	Balance	–
SS	0.08	1.00	1.50	0.03	0.04	18.50	10.20	–	Balance	–
Al	–	0.2	0.05	–	–	–	–	0.05	0.4	Balance

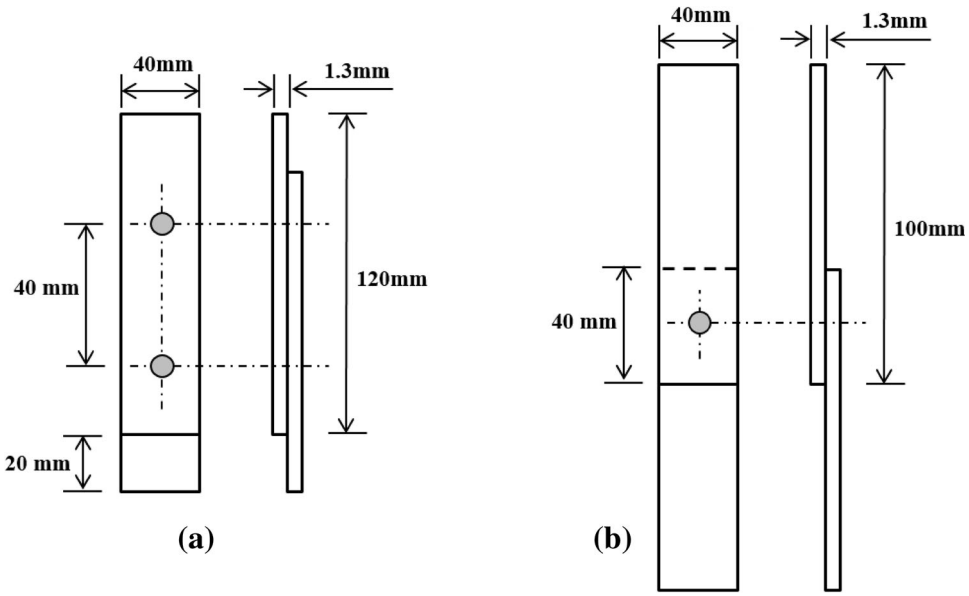

Fig. 2 Dimensions of the **a** peel test, **b** tensile shear test samples

formed at the aluminium/steel interface by the reaction between liquid aluminium and solid/liquid iron which lowers the mechanical performance of the welds. To avoid these issues, the core aluminium is squeezed out before the application of welding current in this work. A "squeeze-out pulse" with a current of 20 kA and duration of 2 cy is applied to melt and squeeze out the aluminium successfully from the clad sheet. After the application of the squeeze-out pulse, the clad sheet behaves like a low carbon steel/stainless steel 2-ply clad sheet as shown in the Fig. 3a. Subsequently, the second pulse, the main "weld pulse", is applied to make a large enough nugget at the sheet/sheet interface. It should be noticed that the terms welding current and welding time used hereafter in this article are the weld pulse current and weld pulse time respectively. The schematic representation of the overall welding schedule is illustrated in Fig. 3b.

Figure 4a shows a fully developed weld nugget with 13 kA welding current and 18 cy welding time. SEM–EDS line scanning has been made in two locations: centre of the nugget and outside the nugget as shown in the Fig. 4b. EDS results also confirm that there is no aluminium left behind in the vicinity of the weld nugget and it has been squeezed completely. Hence, there is no chance of intermetallic compound layer formation at the weld zone.

3.2 Weldability Lobe Diagram

Resistance spot weldability of different materials can be evaluated with different parameters such as weldable current range, electrode tip life [13] and load bearing capacity and fracture mode during mechanical testing [14]. Amongst all, fracture mode is an easy and effective technique for weldability assessment and is the most commonly used qualitative measure of weld quality [7]. The morphology of the fracture is examined during the mechanical testing to ascertain whether the fracture mode is button pull or interfacial fracture. Generally, the welds which exhibit button pull as the fracture mode are considered superior quality welds and the welds which exhibit interfacial fracture are considered inferior quality welds.

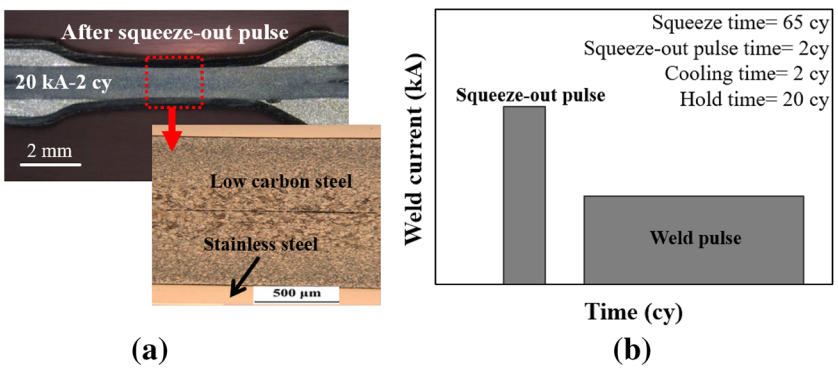

Fig. 3 **a** Cross sectional image of the clad sheet after the application of squeeze-out pulse, **b** a schematic representation of the welding schedule

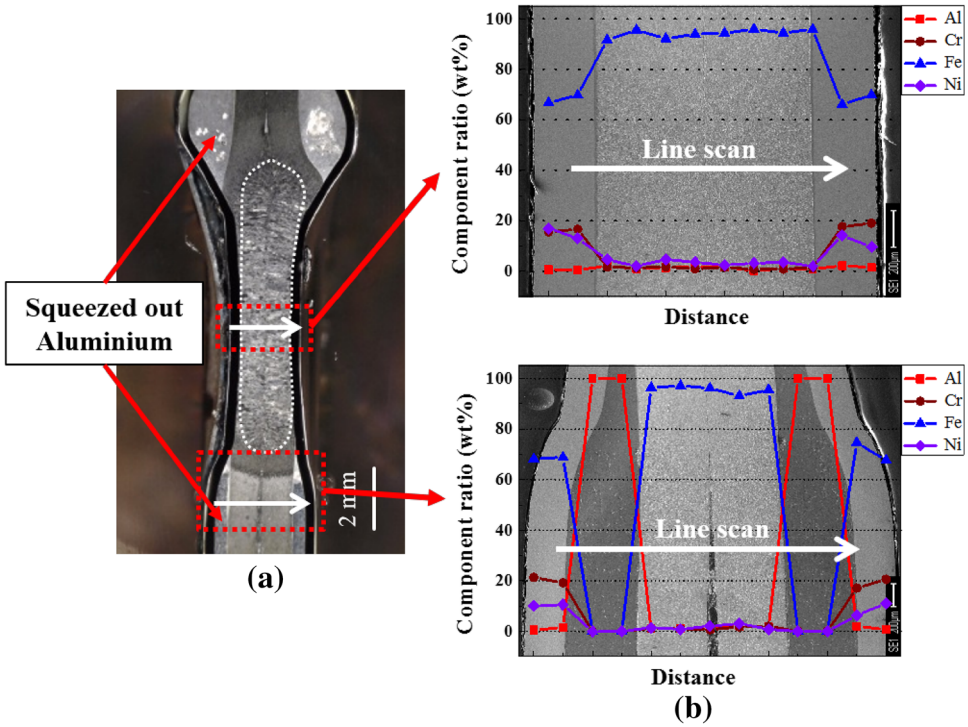

Fig. 4 **a** A fully developed weld nugget (13 kA, 18 cy) which shows the squeeze out of aluminium, **b** SEM–EDS line scanning in two locations: centre of the nugget and outside the nugget where aluminium is squeezed out and entrapped in between the steels

The fracture modes, during the peel test, exhibited by different clad sheet resistance spot welds with an electrode force of 300 kgf, welding current ranging from 10 to 16 kA and welding time ranging from 12 to 20 cy are depicted as a weldability lobe diagram in the time–current space in Fig. 5. A lobe diagram generally contains two boundaries, the acceptable weld size and expulsion. However, in this study, lobe diagram is designed based on the fracture mode and has two boundaries namely acceptable fracture mode, i.e., non-interfacial fracture, and electrode–sheet sticking.

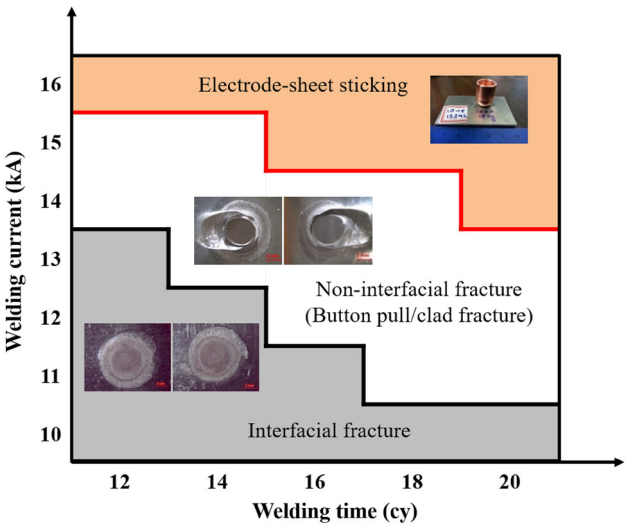

Fig. 5 Weldability lobe diagram based on the fracture modes during peel test

Therefore, the weldability lobe diagram is divided into three regions: interfacial fracture mode region, non-interfacial fracture mode (button pull/clad-bond fracture) region and electrode–sheet sticking region. Electrode–sheet sticking occurs due to the excessive heat generation at the electrode–sheet interface and subsequent bonding of electrode to the sheet. It is strictly an undesirable phenomenon in resistance spot welding process, alike expulsion [13]. Detailed descriptions of different fracture modes are provided in the subsequent sections. It is evident from the lobe diagram (Fig. 5) that the welding time of 18 cy shows the widest weldable current range. Weldable or acceptable current range is nothing but the current range over which the weld exhibits acceptable fracture mode. So, further studies have been carried out with a constant welding time of 18 cy.

3.3 Nugget Diameter and Electrode Indentation

Figure 6 shows the effect of welding current on the weld nugget geometries such as nugget size and degree of electrode indentation in RSW of clad sheet with a constant welding time of 18 cy. At a current of 8 kA, no melting is observed at the sheet to sheet interface, and it is due to the high heat dissipation through the aluminium present in the clad sheet. On increasing the welding current, heat generation is increased, thereby increasing the nugget diameter. "$4\sqrt{t}$" nugget diameter, which is considered as the lower limit of weldable current range [15], is achieved at a welding current of 12 kA. Figure 6 illustrates a uniform

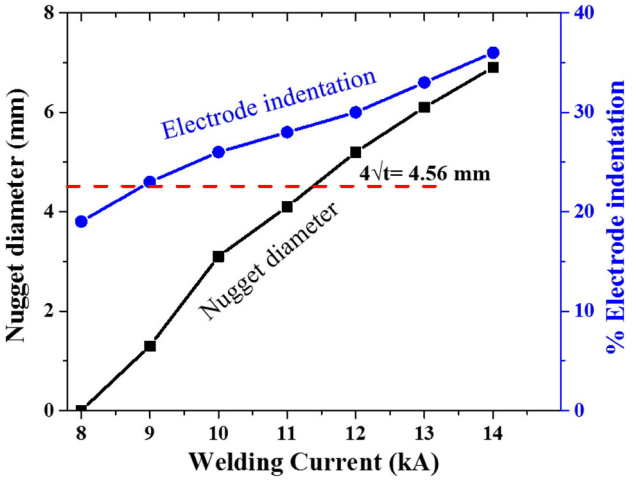

Fig. 6 The effect of welding current on the weld nugget geometries namely nugget size and percentage electrode indentation

increase in percentage electrode indentation with respect to increasing welding current. The degree of electrode indentation basically depends on the heat input during the welding process, and strength and melting point of the material [16]. The outer layer of the clad sheet consists of high strength stainless steel, and is expected to show a low electrode indentation with low heat input. Though, the presence of aluminium causes a high percentage electrode indentation even with a low welding current (heat input), as the aluminium is melted and squeezed out in the early stage of welding.

3.4 Microstructure

Even though the core aluminium is squeezed out of the vicinity of the weld joint, the molten aluminium still reacts with steel and forms an intermetallic compound layer although outside the weld zone. The molten aluminium is squeezed out and entrapped in between the low carbon steel and stainless steel outside the weld zone and reacts with the surrounding steel materials to form intermetallic compound layer as shown in Fig. 7a, b. To reveal the intermetallics formation, detailed images of the presence of intermetallic compound layers in the LCS/Al and SS/Al interface using optical and scanning electron microscopy are provided in Fig. 7c–f. The EDS elemental analysis has been carried out at different points A, B, C and D of Fig. 7d, f and provided in Table 2. It is identified from the EDS elemental analysis, previous research reports and Fe–Al binary phase diagram that the intermetallic layer consists of Fe_2Al_5 and $FeAl_3$ at the LCS/Al interface and $(Fe,Cr,Ni)_2Al_5$ and $(Fe,Cr,Ni)Al_3$ at the SS/Al interface [12]. Usually, the formation of intermetallic reaction layer in the welds is detrimental to the mechanical property of the welds. The brittleness of the intermetallic layer is evident from Fig. 8, which shows a thick intermetallic compound layer with a continuous crack formation. However, the intermetallic layer is formed well outside the weld zone and hence does not affect the joint properties.

3.5 Tensile Shear Test and Fracture Modes

Figure 9 shows the load–displacement diagram during the tensile shear testing of a resistance spot weld made with welding current of 14 kA and welding time of 18 cy. Three different variables are monitored namely peak load, maximum displacement and failure energy during the tensile shear test as shown in Fig. 9. Peak load is the maximum load measured during the testing which indicates the load bearing capacity of the welds, and maximum displacement is the displacement measured at the peak load, which is a measure of the joint ductility. Failure energy is calculated as the area under the load–displacement curve till the peak load, which is the measure of energy absorbed by the specimen during the test and it demonstrates the performance reliability of a weld during impact loading [7, 17].

The tensile shear test results of the joints, plotted as a vertical stack of peak load, maximum displacement and failure energy curves against welding current for a welding time of 18 cy, are shown in Fig. 10. As the welding current increases from 8 to 14 kA, all the monitored variables such as peak load, maximum displacement and failure energy also increases due to increase in nugget size. At 12 kA welding current, a sudden increase in these variables is observed and as a result, an upper shelf in the curves are formed. This is due to the attainment of $4\sqrt{t}$ nugget size and the transition of fracture mode from interfacial fracture mode to non-interfacial fracture mode [15, 18]. It is evident from Figs. 6 and 10, that the welds with nugget diameter less than $4\sqrt{t}$ (=4.56 mm) exhibit interfacial fracture mode and greater than $4\sqrt{t}$ exhibit non-interfacial fracture mode. The fracture mode for each weld is specifically indicated by different symbols in Fig. 10. As per the AWS standard [19], the different fracture modes observed in the current study can be classified as follows.

1. Button pull.
   Figure 11 shows the optical macro-image of the fracture (a and b), schematic diagram of the fracture behaviour (c) and crack propagation (d) of the button pull fracture mode. In this fracture mode, the nugget and base metal of one sheet are removed as a button and is attached to the opposite sheet as shown in Fig. 11a, c. The fracture initiated from the base metal or HAZ, propagates through the thickness of the sheet (Fig. 11d) and leaves behind a hole pulled by the button (Fig. 11b). Button pull is the most desirable

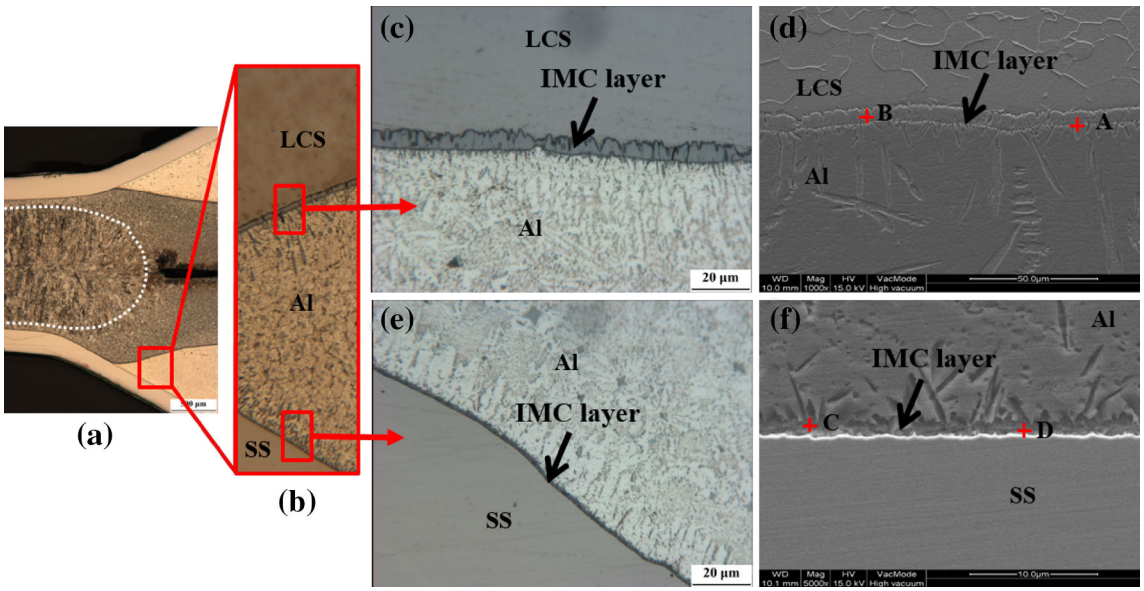

Fig. 7 **a**, **b** Optical micro images showing the location of intermetallic compound layer formation and, optical and SEM images showing the intermetallic compound layer formation at **c**, **d** LCS/Al interface, **e**, **f** SS/Al interface

Table 2 EDS elemental analysis results where A, B, C and D are the corresponding points of analysis in the Fig. 7d, f

Location	Elemental composition of IMC layer (at.%)			
	Al	Fe	Cr	Ni
A	74.81	25.19	–	–
B	69.83	30.17	–	–
C	76.27	22.14	1.26	0.33
D	68.12	29.50	1.97	0.41

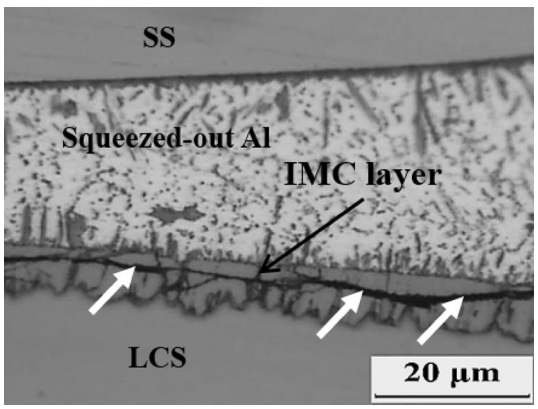

Fig. 8 Optical image showing the crack formation in the intermetallic compound layer

fracture mode as it exhibits the most satisfactory peak load and failure energy values.

2. Clad-bond fracture.

In this fracture mode, the clad-bond between low

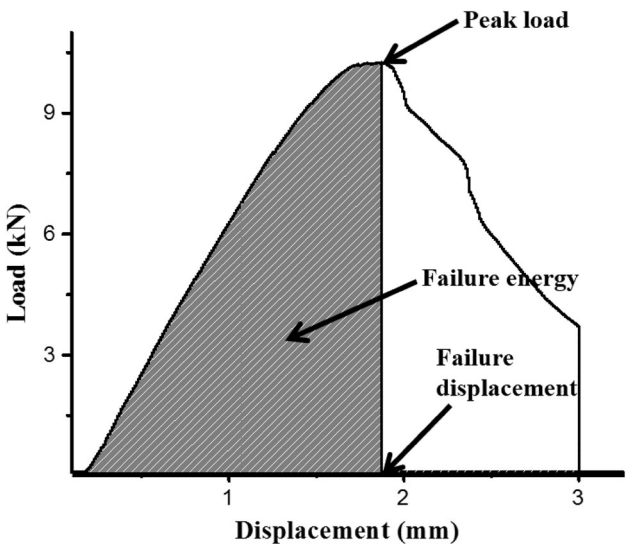

Fig. 9 Load–displacement diagram during tensile shear test of a resistance spot weld with 14 kA and 18 cy

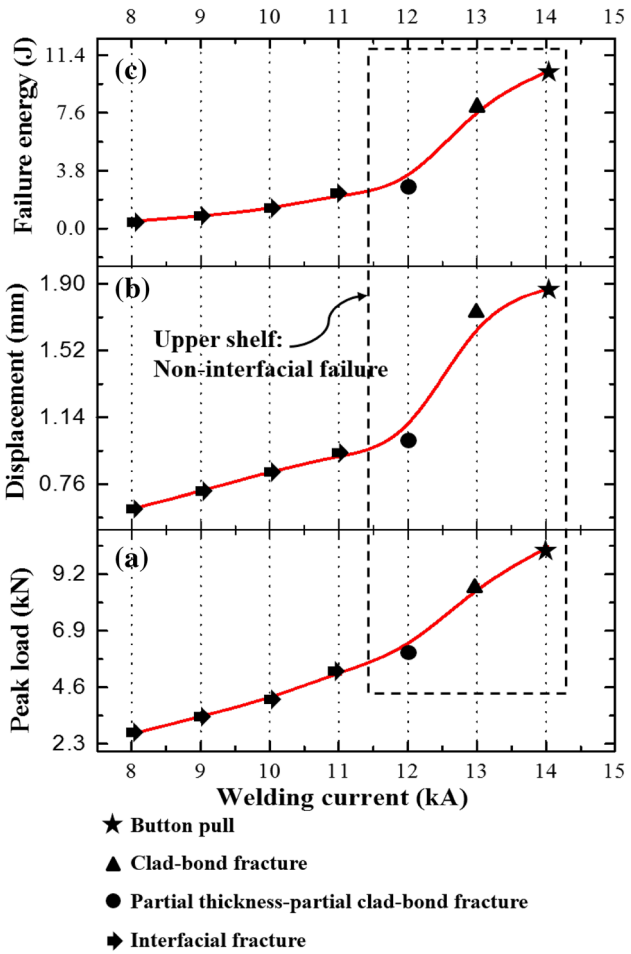

Fig. 10 Tensile shear test results plotted as a vertical stack of peak load, maximum displacement and failure energy curves against welding current

carbon steel and stainless steel is fractured and, the nugget along with the low carbon steel base metal layer of one sheet is removed and is attached to the mating sheet. Figure 12 shows the optical macro-image of the fracture (a and b), schematic diagram of the fracture behaviour (c) and crack propagation (d) of the clad fracture mode. As shown in the figure, the crack initiates from HAZ, propagates into the clad interface and ends up with a cavity in the sheet due to the complete removal of low carbon steel layer.

3. Partial thickness-partial clad-bond fracture.
   It is an incomplete debonding in which slant crack propagates into the fusion zone, clad-bond and part of the low carbon steel layer and is removed during the tensile shear test. Figure 13 shows the optical macro-image of the fracture (a and b), schematic diagram of the fracture behaviour (c) and crack propagation (d) of the partial thickness-partial clad-bond fracture mode.
4. Interfacial fracture.
   This is the most undesirable fracture mode as it exhibits poor performance in service. The fracture propagates through the fusion zone or sheet/sheet interface, resulting in low peak load and failure energy.

During the resistance spot welding of clad sheet, the melting initiates at the LCS/LCS faying interface and forms a small molten nugget and then it enlarges with the weld time. If the weld current is large enough, the nugget will grow into stainless steel layer by melting the clad interface and a portion of stainless steel layer. In case of clad-bond fracture mode or partial thickness-partial clad-bond fracture mode, stainless steel and clad interface are

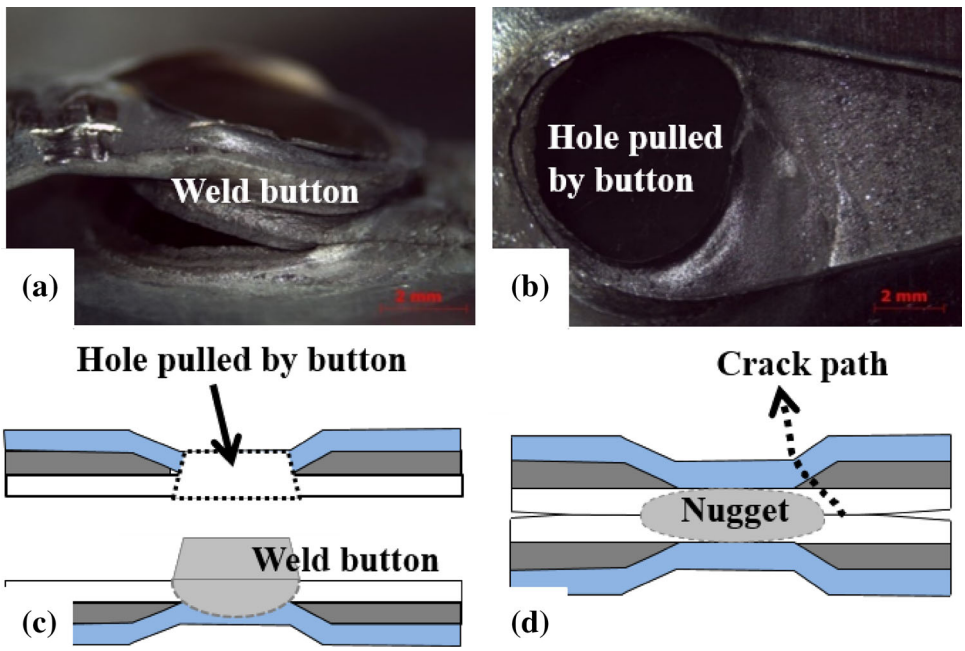

Fig. 11 Button pull fracture: **a** lower sheet, **b** upper sheet, **c** schematic diagram showing the fracture behaviour, **d** schematic diagram showing the crack path

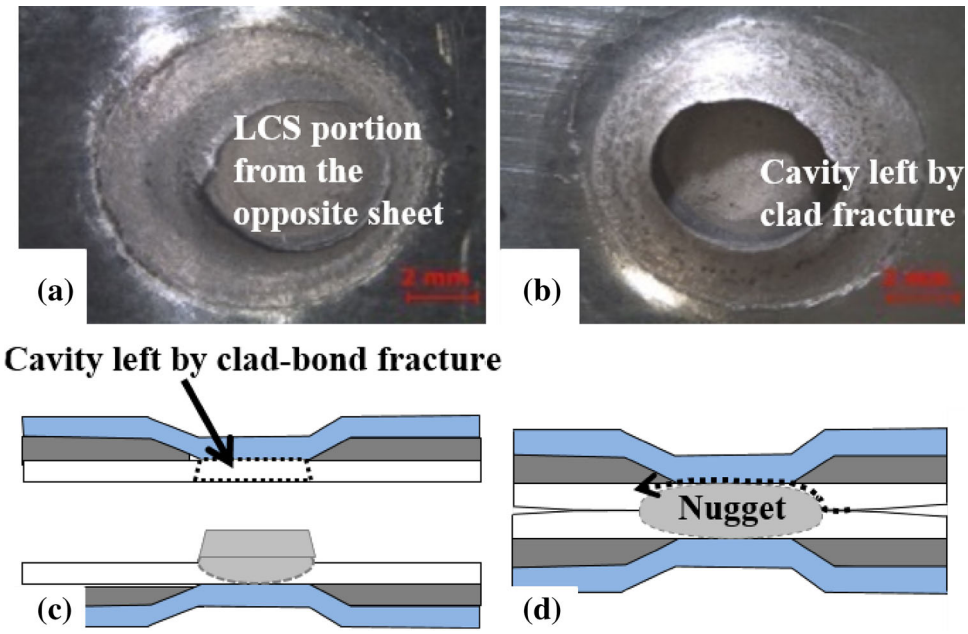

Fig. 12 Clad-bond fracture: **a** lower sheet, **b** upper sheet, **c** schematic diagram showing the fracture behaviour, **d** schematic diagram showing the crack path

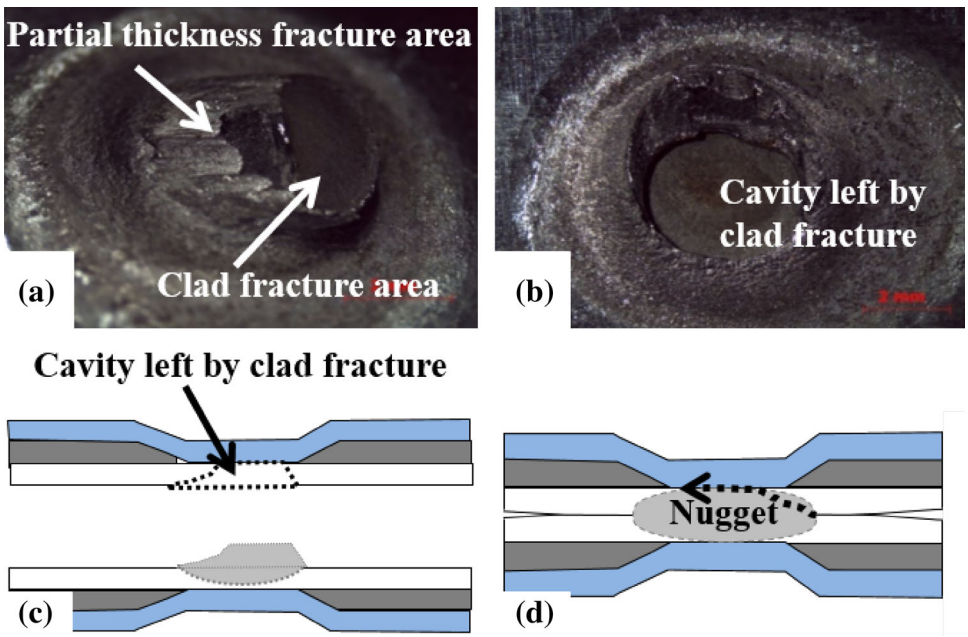

Fig. 13 Partial thickness-partial clad-bond fracture: **a** lower sheet, **b** upper sheet, **c** schematic diagram showing the fracture behaviour, **d** schematic diagram showing the crack path

not melted during the resistance spot welding process as shown in Fig. 14a. Therefore, the crack follows the comparatively weak clad bond. On the other hand, when welds made at high welding current, stainless steel also melts and takes part in the nugget formation. Thus, no clad-bond is observed between stainless steel and low carbon steel as shown in Fig. 14b, c, and consequently the crack propagates into the stainless steel in the direction of its thickness. This causes the button pull fracture in resistance spot welds of clad sheet with high welding current. The fracture characteristics of clad sheet resistance spot welds with respect to welding current within the experimental conditions are analysed and the results are summarized in Fig. 15. At first, the fracture mode transforms from interfacial fracture to clad-bond or partial thickness-partial clad-bond fracture due to the attainment of "$4\sqrt{t}$" nugget size and then transforms to button pull fracture due to the melting of the clad interface and the stainless steel layer. Thus, the nugget size and melting of clad interface and stainless steel layer are the dominant factors in determining the fracture mode.

Previous studies have revealed that fracture mode significantly affects the load bearing capacity (peak load) and energy absorption (failure energy) of spot welds [17].

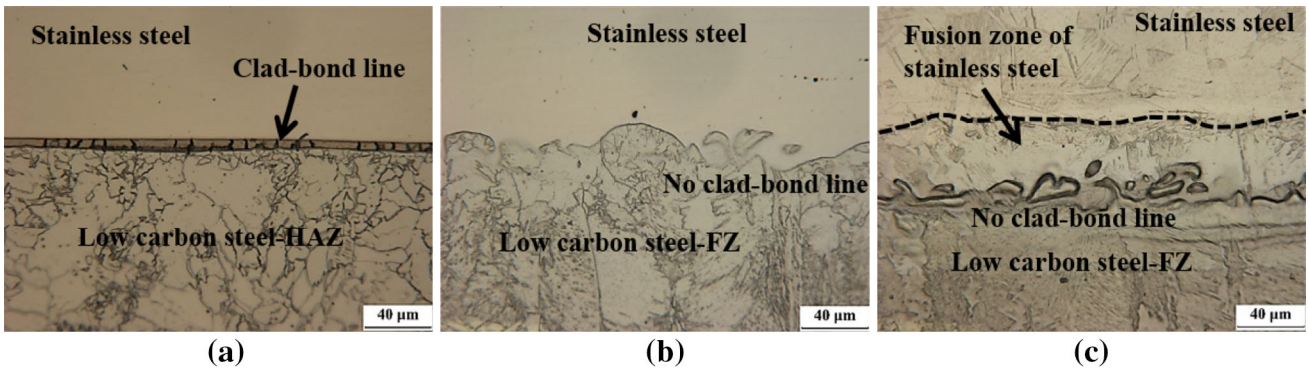

Fig. 14 Optical micro images of LCS/SS interface of weld with 12 kA showing clad interface (**a**), weld with 14 kA showing melted stainless steel layer and disappeared clad interface (**b**, **c**)

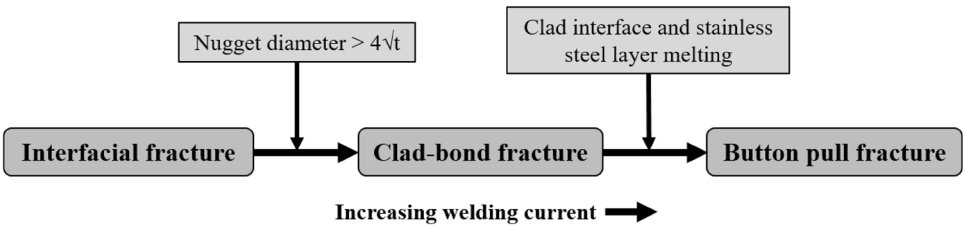

Fig. 15 Summary of the fracture characteristics of resistance spot welded clad sheets

Normally, button pull fracture is considered as the preferred fracture mode owing to its higher load bearing capacity, displacement at failure and energy absorption during the tensile shear test of resistance spot welds. The results of tensile shear tests of clad sheet resistance spot welds are in good agreement with the above statement. The weld with button pull fracture exhibits a peak load of 10.2 kN and a failure energy of 10.5 J. At the same time, the weld exhibiting clad-bond fracture shows a peak load of 8.7 kN and a failure energy of 8.2 J. When the fracture mode is changed from button pull to clad fracture, peak load decreases by 14.7% and failure energy decreases by 21.9%. However, the peak load and failure energy associated with clad fracture are still significantly high enough for the practical applications of the resistance spot welds of clad sheets.

4 Conclusions

The weldability, microstructure, mechanical properties and fracture behaviour of the resistance spot welded LCS/Al/SS 3-ply clad sheets were examined and the following conclusions were obtained.

1. The core aluminium was melted and squeezed out completely by applying a "squeeze-out pulse" before the application of actual welding current. It enabled the clad sheet to weld with no Fe–Al intermetallic compound layer formation in the weld zone.
2. A weldability lobe diagram based on the fracture mode during the peel test was constructed and consisted of three regions namely the interfacial fracture mode region, the non-interfacial fracture (button pull/clad-bond fracture) mode and the electrode–sheet sticking region. Non-interfacial fracture region was considered to be the acceptable weld region and a welding time of 18 cy exhibited the widest weldable current range.
3. The squeezed out molten aluminium reacted with the surrounding steel and formed continuous intermetallic compound layer outside the nugget. As the intermetallic compound layer was formed well outside the weld zone it did not affect the joint properties.
4. With increasing welding current, all the monitored variables (the peak load, the maximum displacement and the failure energy) during the tensile shear test increased due to increasing nugget size.
5. The fracture behaviour examinations revealed four different fracture modes: (1) button pull; (2) clad-bond fracture; (3) partial thickness-partial clad-bond fracture; (4) interfacial fracture. Accomplishment of "$4\sqrt{t}$" nugget size caused the fracture mode transformation from interfacial to clad-bond fracture while the melting of the clad interface and the stainless steel layer caused the fracture mode transformation from clad-bond/partial-thickness partial clad-bond to button pull fracture. In other words, nugget size and melting of clad interface and stainless steel layer were the dominant factors in determining the fracture mode.

References

1. Mori T, and Kurimoto S, *J Mater Process Technol* **56** (1996) 242.
2. Okui T, Yonemitsu Y, and Yoshida K, *Development of Metal Clad Sheets and Strips*, Technical Report No. 106, Nippon Steel & Sumitomo Metal (2014).
3. Lee J L, Bae D H, Chung W S, Kim K H, Lee J H, and Cho Y R, *J Mater Process Technol* **187** (2007) 546.
4. Tricarico L, and Spina R, *Mater Des* **31** (2010) 1981.
5. Rhee K Y, Han W Y, Park H J, and Kim S S, *Mater Sci Eng A* **384** (2004) 70.
6. Macwan A, Patel V K, Jiang X Q, Li C, Bhole S D, and Chen D L, *Mater Des* **62** (2014) 344.
7. Zhang H, and Senkara J, *Resistance Welding: Fundamentals and Applications*, CRC Press, New York (2006) p 19.
8. Missori S, Murdolo F, and Sili S, *Weld J* **83** (2004) 65s.
9. Yoon J S, Lee S H, and Kim M S, *J Mater Process Technol* **111** (2001) 85.
10. Oikawa H, Ohmiya S, Yoshimura T, and Saitoh T, *Sci Technol Weld Join* **4** (1999) 80.
11. Sun X, Stephens E V, Khaleel M A, Shao H, and Kimchi M, *Weld J* **83** (2004) 188S.
12. Qiu R, Iwamoto C, and Satonaka S, *J Mater Process Technol* **209** (2009) 4186.
13. Zhou Y, Gorman P, Tan W, and K. Ely K J, *J Electron Mater* **29** (2000) 1090.
14. Lim S S, Kim Y T, Chun E J, Nam K S, Park Y W, Kim J W, Lee S Y, and Choi I D, *J Weld Join* **34** (2016) 1.
15. Sun X, Stephens E V, and Khaleel M A, *Weld J* **86** (2007) 18s.
16. Hayat F, *Mater Des* **32** (2011) 2476.
17. Pouranvari M, and Marashi S P H, *Sci Technol Weld Join* **18** (2013) 361.
18. Marashi S P H, Pouranvari M, Amirabdollahian S, Abedi A, and Goodarzi M, *Mater Sci Eng A* **480** (2008) 175.
19. AWS, *Specification for Automotive Weld Quality: Resistance Spot Welding of Steel* (2007).